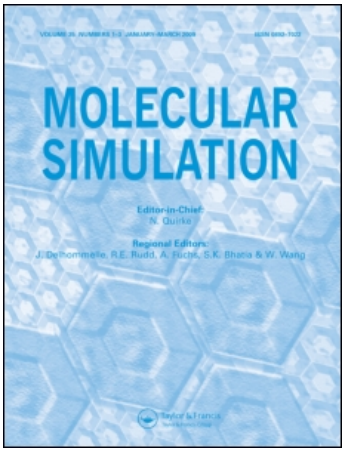

Molecular Simulation
Publication details, including instructions for authors and subscription information:
http://www.informaworld.com/smpp/title~content=t713644482

Computational investigation of pressure profiles in lipid bilayers with embedded proteins

J. Gullingsrud[a]; A. Babakhani[a]; J. A. McCammon[ab]
[a] Department of Chemistry and Biochemistry, University of California, San Diego, CA, USA [b] Department of Chemistry and Biochemistry, Howard Hughes Medical Institute, University of California, San Diego, CA, USA

To cite this Article Gullingsrud, J. , Babakhani, A. and McCammon, J. A.(2006) 'Computational investigation of pressure profiles in lipid bilayers with embedded proteins', Molecular Simulation, 32: 10, 831 — 838
To link to this Article: DOI: 10.1080/08927020600779350
URL: http://dx.doi.org/10.1080/08927020600779350

Molecular Simulation, Vol. 32, Nos. 10–11, 30 August–15 September 2006, 831–838

Taylor & Francis
Taylor & Francis Group

Computational investigation of pressure profiles in lipid bilayers with embedded proteins

J. GULLINGSRUD†*, A. BABAKHANI†¶ and J. A. McCAMMON†‡§

†Department of Chemistry and Biochemistry, University of California, 9500 Gilman Drive, MC-0365, La Jolla, San Diego, CA 92093-0365, USA
‡Department of Chemistry and Biochemistry, Howard Hughes Medical Institute, University of California, 9500 Gilman Drive, MC-0365, La Jolla, San Diego, CA 92093-0365, USA

(Received January 2006; in final form May 2006)

The distribution of surface tension within a lipid bilayer, also referred to as the lateral pressure profile, has been the subject of theoretical scrutiny recently due to its potential to radically alter the function of biomedically important membrane proteins. Experimental measurements of the pressure profile are still hard to come by, leaving first-principles all-atom calculations of the profile as an important investigative tool. We describe and validate an efficient implementation of pressure profile calculations in the molecular dynamics package NAMD, capable of distinguishing between internal, bonded and nonbonded contributions as well as those of selected atom groups. The new implementation can also be used in conjunction with Ewald summation for long-range electrostatics, improving the accuracy and reproducibility of the calculated profiles. We then describe results of the calculation of a pressure profile for a simple protein–lipid system consisting of melittin embedded in a DMPC bilayer. While the lateral pressure in the protein–lipid system is nearly the same as that of the bilayer alone, partitioning of the lateral pressure by atom type revealed substantial perturbation of the pressure profile and surface tension in an asymmetric manner.

Keywords: Lipid bilayer; Melittin; Pressure profile; Protein–lipid interactions

1. Introduction

Lipid bilayers are the dominant structural component of cellular membranes. However, the diversity of lipids expressed in cells as well as their specific localization reflects their active role in determining the propensity of peptides to insert into bilayers, as well as the activity and function of integral membrane proteins. While protein–lipid interactions occur via a number of modes, including direct hydrogen bonding and specific interactions with the transmembrane portion of membrane proteins, the role of chemically non-specific lateral pressures has become increasingly well appreciated in recent years.

At equilibrium, cellular lipid bilayers are found in a tension-free state. Yet, the internal membrane lateral pressure, which stems from the interactions of membrane constituents, can vary significantly according to depth in the bilayer as well as the lipid composition [1]. This variation is attributable to a complex interplay of interactions between lipid components and the surrounding solvent, including the repulsion of the phosphate headgroups (a positive pressure), the hydrophobic–hydrophilic interface (a negative pressure) and the entropic repulsion of the hydrocarbon tails (a positive pressure) [2]. The profile could be expected to be even more complex in the presence of transmembrane proteins, which make up a significant portion of many lipid bilayers *in vivo*.

While some progress has been made in directly measuring the lateral pressures in bilayers [3], computational approaches are still an important tool for investigating the nature of the pressure distributions and their dependence on membrane composition. Both statistical models [2], coarse-grained molecular dynamics (MD) [4,5], and all-atom MD [6,7] have been used to directly calculate the lateral pressure from the underlying molecular interactions. The MD approach, while much more computationally intensive than more coarse-grained approaches, benefits from the decades-long development of transferable force fields as well as the ability to model specific lipid headgroups and protein inclusions in atomic

*Corresponding author. Tel: 1-858-534-2905. Fax: 1-858-534-4974. Email: jgulling@mccammon.ucsd.edu
¶Email: ababakha@mccammon.ucsd.edu
§Email: jmccammon@ucsd.edu

Molecular Simulation
ISSN 0892-7022 print/ISSN 1029-0435 online © 2006 Taylor & Francis
http://www.tandf.co.uk/journals
DOI: 10.1080/08927020600779350

detail. An all-atom approach thus presents the opportunity to develop a consistent model of both specific, chemical interactions between lipids and proteins, as well as non-specific, physical effects such as those arising from inhomogeneous distributions of, and shifts in, lateral pressures.

Recent experimental results seem to suggest that, while specific lateral pressure profiles play a role in modulating membrane protein behavior in some cases, specific lipid–protein interactions are still critical for function. An illustrative example is the interaction of the nicotinic acetylcholine receptor (nAchR) with its surrounding lipid environment. Solid-state NMR measurements suggest a strong interaction between the αm1 segment of nAchR and dimyristoylphosphatidylcholine (DMPC) bilayers, leading to effects on lipid organization that cannot be explained solely by hydrophobic mismatch or bilayer rigidity [8]. Contrary to physical mechanisms of membrane protein control, it was found by Martinez *et al.* [9] that nAchR exhibits binding kinetics in a complex of amphipathic polymers similar to that of its native membrane environment [9]. However, in detergent, the kinetic properties of the channel are markedly different. The authors argue that the data supports a molecular mechanism of channel function modulation, rather than a generic, physical mechanism. Baenzinger *et al.* find mixed results [10]: either dioleoylphosphatidic acid (DOPA) or cholesterol in a reconstituted egg phosphatidylcholine membrane can influence the equilibrium between nAchR states, but anionic lipids are required for nAchR to adopt a fully functional conformation.

The present work seeks to extend lateral pressure calculations to protein–lipid systems. For comparison with previous work we chose to model a well-studied peptide, melittin, which forms stable helices and aggregates in bilayers. Pressure profiles for membrane proteins have been studied previously [11,12], to our knowledge no protein–lipid systems have been studied in this manner using all-atom MD. The effect of lateral pressures on a system as simple as a single helical peptide ought to be discernable in simulation, as thermodynamic transfer energies for insertion of helices of varying composition have been shown to depend on the location of residues within the polypeptide chain [13].

Consisting of 26 amino acids, melittin embeds itself in cellular membranes, disrupts their integrity and eventually leads to lysis. The mechanism of such embedment as well as the orientation of melittin in the lipid bilayer are the subjects of much research. It has long been suggested that melittin can lie either laterally across the membrane or insert itself parallel to the lipid normal, with the hydrophilic carboxy terminus protruding out of the membrane [14]. A computational study of the former orientation demonstrating its stability has been presented [15].

The present article introduces preliminary findings of a computational study of the latter orientation of melittin (parallel to the normal) in a lipid bilayer. In particular, we seek to calculate the lateral pressure profile of a DMPC bilayer hosting melittin in the normal-parallel orientation and to contrast this to a profile of the membrane without melittin. The objective is to demonstrate a significant difference between the pressure profiles of the membrane-protein and no-protein complexes. If such a difference exists, one can then study the effect of the protein-altered pressure profile on other constituents (possibly other proteins) in the membrane.

2. Theoretical methods

2.1 Construction and equilibration of simulation systems

The DMPC system was based on a pre-equilibrated membrane from the Tieleman laboratory (http://www.ucalgary.ca/~tieleman/download.html). The melittin coordinates used were those of 2MLT.pdb, downloaded from the Protein Data Bank [16]. The DMPC membrane originally contained 128 lipids (divided evenly between the top and bottom monolayers), was solvated with 3655 water molecules and previously equilibrated for 1 ns at a constant area of 0.596 nm^2/lipid. The membrane normal was oriented with the z-axis.

Using the visual molecular dynamics (VMD) program [17] and in a manner similar to that of Bachar *et al.* [18], three DMPC residues near the center of the membrane were deleted from the bottom monolayer, as well as four from the top monolayer. The melittin structure, stripped of its sulfate ions, was carefully placed along the z-axis in this cavity; see Figure 1. After neutralization, this new system, which we refer to as DMPC + Mel, consisted of 121 DMPC lipids (61 in the bottom monolayer,

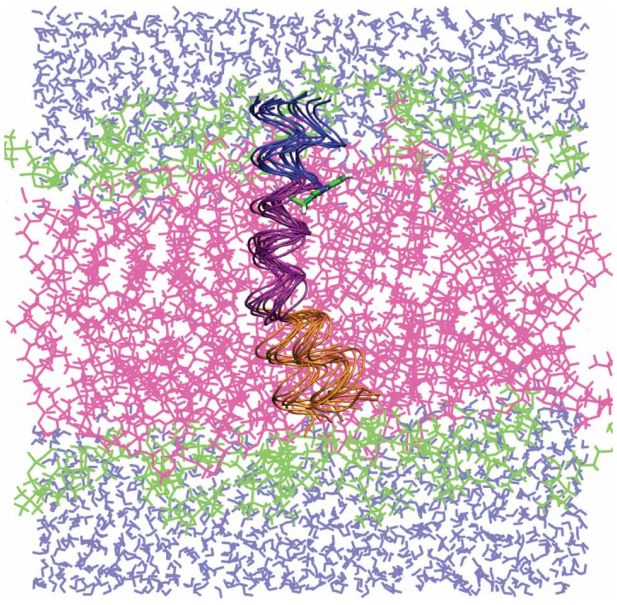

Figure 1. Intial snapshot of melittin-DMPC system, colored by atom type used in the pressure profile analysis: lipid headgroups (green), lipid tails (pink), water (light blue), Melittin residues 1–11 (orange), 12–20 (purple), and 21–26 (dark blue). Melittin conformations are shown from snapshots separated by 2 ns. See online version for colour.

60 in the top), the 26-residue melittin, five chloride ions and 3637 TIP3 water molecules for a total of 25,625 atoms. Following a 5 ps equilibration period, pressure profile data was gathered under conditions identical to equilibration from runs of 14.3 ns for the DMPC system and 22.08 ns for the DMPC + Mel system.

The molecular dynamics program NAMD [19] with the CHARMM27 force field [20] was employed for all MD simulations and calculations. Following the procedure of Berneche *et al.* [15], the system was equilibrated at 330 K, with temperature control provided by Langevin dynamics with a coupling constant of $2\,\mathrm{ps}^{-1}$, and pressure control via the Langevin piston method [21]. The cross-sectional area of the membrane was held fixed at 59.4 by 63.0 Å, while the pressure normal to the bilayer was maintained at 1atm. Bonds to hydrogens were fixed, permitting a timestep of 2 fs. Nonbonded interactions were smoothly switched off between 9 and 10 Å. Long-range electrostatic forces were evaluated using the particle mesh Ewald (PME) method [22] with grid spacing less than 1 Å along each axis.

The pressure profile was further partitioned by atom type (see below). The partition for the melittin system is shown in Figure 1. Besides lipid and solvent atoms, we partitioned the melittin peptide into three segments, which we refer to as Mel (1–11), Mel (12–20), and Mel (21–26), corresponding to the residues included in each partition.

2.2 Pressure profile implementation

The bulk pressure P is expressed in terms of the contributions made by kinetic and inter–particle interactions as

$$P = \frac{1}{\Delta V}\left[\sum_i m_i \mathbf{v}_i \otimes \mathbf{v}_i - \sum_{ij} F_{ij} \otimes r_{ij}\right], \qquad (1)$$

where V is the volume, m_i and $\mathbf{v}_i$ are the mass and velocity of the ith particle, F_{ij} and r_{ij} are the interaction force and distance between particles i and j. Calculation of the lateral pressure profile requires partitioning into several different spatial regions. At equilibrium the off-diagonal elements of P vanish, and in a homogeneous system such as bulk solvent the diagonal components will be equal. Anisotropic systems such as lipid bilayers may maintain a nonvanishing surface tension γ, given by

$$\gamma = \int_{-h/2}^{h/2} \mathrm{d}z \left[P_{zz} - \frac{1}{2}(P_{xx} + P_{yy})\right] \qquad (2)$$

where $2h$ is the total bilayer thickness (with the membrane center placed at 0), and the latter quantity in the integrand is the lateral pressure [6]. The integration takes place over the entire simulation space.

We consider here systems with anisotropy only along one axis, which we assign to z, so that the system may be partitioned into "slabs" perpendicular to the z-axis. Calculation of the spatial distribution of the lateral pressure requires that the contributions to the virial be somehow distributed over the several slabs. A natural choice of contour, employed by several previous efforts [6,7,11], is the Irving–Kirkwood contour [23], in which the contribution from each interaction is distributed evenly between slabs lying on a straight line between the interacting particles. It has been pointed out, however [24], that this approach is limited to describing pairwise interactions, which precludes the use of common electrostatics methods such as PME in the computation of the pressure profile. PME can be reasonably well approximated using long cutoffs [24], but artifacts may still remain due to the non-uniform distribution of charges in the plane of the bilayer and the slow convergence of the distribution of lipids.

Using a different contour, known as the Harasima contour [25], full electrostatics can readily be employed in the pressure profile calculation by using Ewald sums [24]. At sufficiently high accuracies, the Ewald sum and the particle mesh ewald computation converge to precisely the same result. PME has the advantage of converging faster and producing smooth forces, which are required for MD simulation.

For the purpose of determining the contributions of water, lipid, protein, or other classifications of atom types to the pressure profile, we also computed pressure profiles decomposed by atom type. Following the notation of Essman *et al.* [22], the reciprocal space contribution to the electrostatic energy E_{rec} of a configuration of N charged particles with coordinates $\{\mathbf{r}_i\}$ is given by

$$E_{\mathrm{rec}} = \frac{1}{2\pi V}\sum_{\mathbf{m}\neq 0} \frac{\exp(-\pi^2\mathbf{m}^2/\beta^2)}{\mathbf{m}^2} S(\mathbf{m})S(-\mathbf{m}), \qquad (3)$$

where the structure factor $S(\mathbf{m})$ is given by

$$S(\mathbf{m}) = \sum_{j=1}^{N} q_j \exp(2\pi i \mathbf{m}\mathbf{r}_j) \qquad (4)$$

and the reciprocal lattice vectors $\mathbf{m} = m_1\mathbf{b}_1 + m_2\mathbf{b}_2 + \mathbf{b}_1 + m_2\mathbf{b}_2 + m_3\mathbf{b}_3$ for integers m_1, m_2 and m_3 not all zero. For the purpose of obtaining a pressure profile, one simply expands one of the structure factor terms in equation (4) and rearranges the order of summation to obtain the contribution of the pressure provided by each individual atom:

$$V\Pi^i_{\mathrm{rec}\alpha\beta} = \frac{q_i}{2\pi V}\sum_{\mathbf{m}\neq 0} f_{\alpha\beta}(\mathbf{m})\mathrm{Re}\left[\exp(-i\mathbf{m}.\mathbf{r}_i)S(\mathbf{m})\right] \qquad (5)$$

where we have defined

$$f_{\alpha\beta}(\mathbf{m}) \equiv \frac{\exp(-\pi^2\mathbf{m}^2/\beta^2)}{\mathbf{m}^2} \times \left(\delta_{\alpha\beta} - 2\frac{1+\pi^2\mathbf{m}^2/\beta^2}{\mathbf{m}^2}\mathbf{m}_\alpha\mathbf{m}_\beta\right) \qquad (6)$$

where α and β are the unit cell vector and conjugate vectors (respectively), and $\delta_{\alpha\beta}$ is the Kronecker delta (if $\alpha = \beta$, $\delta_{\alpha\beta} = 1$, otherwise $\delta_{\alpha\eta} = 0$).

The particle mesh Ewald method proceeds by interpolating the structure factor onto a grid. Although it seems that the pressure profile could in principle be determined directly from the PME approximation to the structure factor, such an expression is much more unwieldy than the direct Ewald sum. Moreover, since (as described below) the Ewald contribution may be calculated offline, and plays no role in the simulation dynamics, the calculation of the Ewald contribution need not be as fast as PME.

The Ewald sum also admits a partition into contributions from selected atom types. If the structure factor equation (4) is decomposed into k partitions $S_1(\mathbf{m}) + S_2(\mathbf{m}) + \ldots + S_k(\mathbf{m})$, then, from equation (3), the reciprocal energy can be written

$$E_{\text{rec}} = \sum_{s=1}^{k} E_{\text{rec},s} + \sum_{s \neq t} \sum_{\mathbf{m} \neq 0} \frac{\exp(-\pi^2 \mathbf{m}^2 / \beta^2)}{\mathbf{m}^2} S_s(\mathbf{m}) S_t(-\mathbf{m}) \quad (7)$$

where E_s is the reciprocal space energy if only particles of type s are considered. The remaining cross terms can be considered to arise from the interactions between particles of type s and t, and can themselves be spatially partitioned just as was done for interactions between atoms of the same type.

In the new NAMD implementation, all contributions to the pressure profile except the Ewald sum are computed "online"; that is, as the simulation proceeds. For each pressure profile slab, the module outputs the average of the pressure tensor for all timesteps since the previous output. This self-averaging improves the convergence of the nonbonded contribution to the pressure profile and avoids problems associated with using multiple timestepping [7]. In addition to the total pressure profile, the contributions from "internal", "bonded", and "nonbonded" are output separately. "Internal" incorporates contributions from the kinetic energy of the particles, as well as correction forces arising from rigid bond constraints. The "bonded" portion contains the usual covalent terms present in the force field, while "nonbonded" contains all van der Waals and electrostatic interactions.

If multiple atom types have been specified, all three contributions to the pressure profile are further subdivided by atom type. One set of "internal" contributions are reported for each atom type. For "bonded" and "nonbonded", the self interactions of each atom type with other atoms of the same type, as well as the pairwise interactions of each atom type with every other atom type, are recorded. In the current implementation, up to 15 different atom types can in principle be analyzed simultaneously.

If a simulation was conducted using PME for electrostatics, a second offline calculation needs to be made to account for the reciprocal space contribution to the pressure. In the previous implementation (present in NAMD 2.5), this could be done only by setting a long cutoff. In the new implementation, the PME contribution can be estimated using a cutoff as before (by ignoring the nonbonded contribution in the online calculation and re-computing the nonbonded contribution using a long cutoff), or with the Ewald summation method.

The calculations presented here all used the Ewald sum for the calculation of the pressure profile. The maximum Ewald k-vector along each direction was sixteen; no significant improvement was observed when more k-vectors were added.

3. Results

The distribution of melittin residues within the DMPC bilayer is shown in Figure 2(A). While the N-terminal half of the peptide lies entirely within the hydrophobic core of the bilayer, much of the C-terminal region resides in the solvent-headgroup interface region. That this region (and specifically residue 19, tryptophan) remains in the interface during the entire simulation agrees well with previous experimental and simulation results [26,18]. A small kink in the helix is reflected in a change in slope of the melittin residue distribution at Gly12. This kink, as well as the overall disposition of the melittin within the bilayer, remained fairly constant for the duration of the simulation. Such observations are characteristic of melittin-membrane simulations [18].

We computed lateral pressure profiles for both the DMPC and DMPC + Mel systems. For purposes of comparison, we also computed the pressure profile for the DMPC + Mel system with the contributions from melittin atoms excluded from the sum. We refer to this "virtual" system as DMPC + ExcMel. The lateral pressure profiles computed from the DMPC, DMPC + Mel and DMPC+ExcMel simulation are shown in Figure 2(B). As in previous work [7], the peak tension, corresponding to minimum lateral pressure, lies just inside the average depth of the phosphate groups of the bilayer. In both simulations the profile is reasonably symmetric, and drops to zero in the water phase, indicating that the bilayer is sufficiently hydrated.

While the total pressure profile in the DMPC and DMPC + Mel simulations appears very similar, the contribution to the lateral pressure made by the lipid alone is substantially offset in the upper monolayer by the contribution made by the melittin. Only a small change in the profile of the DMPC + Mel simulation compared to the pure DMPC simulation is observed in the lower leaflets. As seen in Table 1, the total tension in the membrane is nearly the same in the two systems, differing by less than the statistical error in their measurement. Although the area per lipid and lipid order parameter

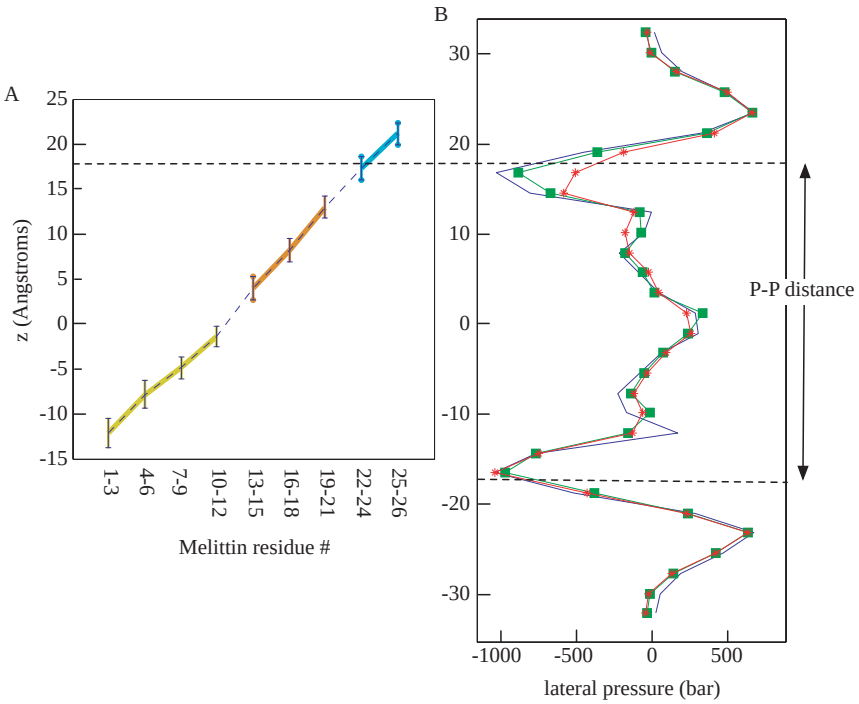

Figure 2. (A) Distribution of melittin residues within the bilayer. (B) Lateral pressure profile computed from DMPC-only simulation (DMPC blue), DMPC with melittin (DMPC + Mel, green), and DMPC with melittin but excluding the contribution of melittin interactions (DMPC + ExcMel, red) in online version.

(Figure 4) in our simulations are in good agreement with experimental membrane values [27], the system still exhibits positive surface tension. This is in agreement with previous work employing the CHARMM parameter set for lipids [28], where it was found that a surface tension of 35–45 dyne/cm gave the best agreement with known area per lipid. Our smaller tensions in the range of 10–20 dyne/cm probably derive from the larger size of the bilayers in our simulations (60 lipids per monolayer, compared to 36 in Ref. [28]).

The tension computed from the pressure profile analysis will necessarily differ slightly from the tension computed on the fly during the respective simulations, simply because it is based in part upon post-processing of trajectory timesteps sampled 500 ps apart. As seen in table 1, the tensions computed from the pressure profiles are both well within the statistical error of the direct simulation values. However, the pressure profile analysis also reveals that the tensions in the individual monolayers are nearly the same in the DMPC simulation, but differ substantially in the DMPC + Mel simulation. The tension in the lower leaflet is nearly 5 dyne/cm larger than in pure DMPC, and 4 dyne/cm smaller in the upper leaflet. This is despite the fact that, in the construction of the DMPC + Mel system, the upper leaflet has fewer lipids than the lower leaflet (60 vs. 61, respectively); thus, if the two termini of melittin were perfectly symmetric, one would expect that the upper leaflet would exhibit greater tension due to its increased area per lipid. In fact, the opposite is observed, suggesting that protein–lipid interactions are the primary mechanism responsible for decreasing the tension in the upper leaflet and increasing the tension in the lower leaflet.

The asymmetry in the tension is even more striking when melittin interactions are excluded from the calculation. Values in the third line of table 1 are computed for contributions to the pressure profile from lipid, water, and interactions between lipid and water. The average tension in the DMPC + Mel system when melittin is excluded is only 8 dyne/cm, compared to 13.3 dyne/cm for the complete system. Yet, the computed tension in the lower leaflet is even greater than in the complete DMPC + Mel system, 19.2 vs. 18 dyne/cm, while the tension in the upper leaflet is much smaller, 3.2 vs. 8.5 dyne/cm.

Despite the large difference in tension between the two leaflets, the available area per lipid is not substantially

Table 1. Per-monolayer tension computed, respectively, from total virial during the simulations, from the pressure profile, and from the pressure profile for the lower and upper leaflets separately. All units are in dyne/cm. See the caption of Figure 2 for definitions of abbreviations.

	Pressure tensor	*Pressure profile*	*Lower leaflet*	*Upper leaflet*
DMPC	12.2 ± 1.4	12.7	12.9	12.6
DMPC + Mel	13.2 ± 1.1	13.3	18.0	8.5
DMPC + ExcMel	N/A	8.0	19.2	3.2

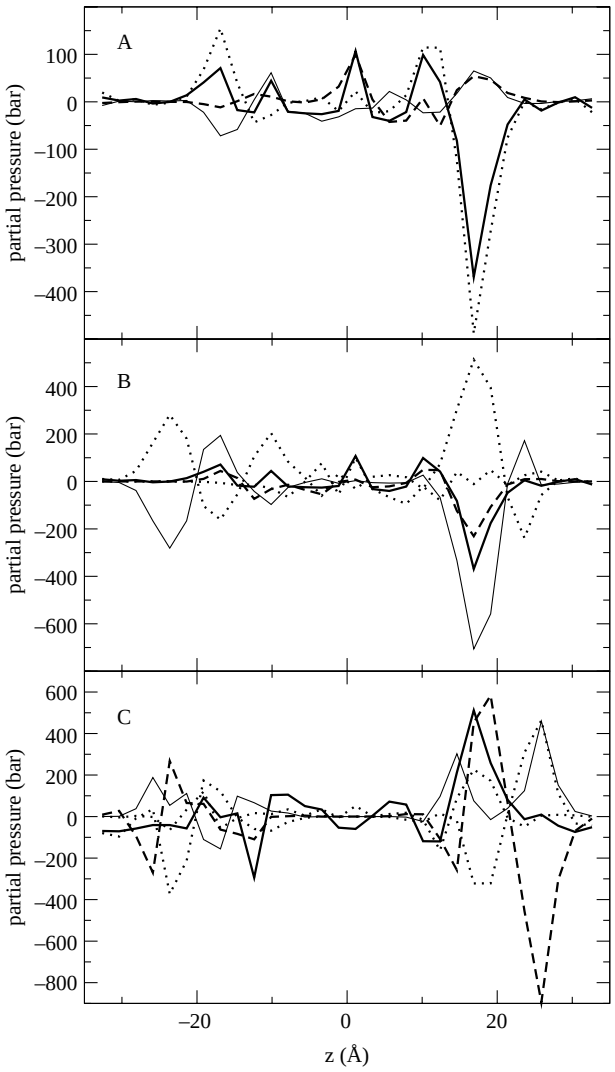

Figure 3. (A) Partial pressures of melittin: contribution from complete protein(thick solid line); melittin residues 1–11(thin solid line); residues 12–20(dashed line); residues 21–26(dotted line). (B) Partial pressures arising from interactions of melittin with other simulation components. Thick solid line: total melittin pressure; thin solid line: interactions with lipid headgroups; dashed line: interactions with lipid tails; dotted line: interactions with water; dot-dashed line: interaction with self. (C) Difference between pressure profile components in DMPC + melittin simulation and pure DMPC simulation. Thick solid line: total difference in membrane + water contribution to the pressure profile; thin solid line: headgroup–headgroup interactions; dashed line: headgroup–water interactions; dotted line: tail–water interactions; dot-dashed line: water–water interactions.

different, and thus, as shown Figure 4(A), the lipid order parameter in the two leaflets is virtually indistinguishable. This similarity in order parameter between the two leaflets has also been noted in previous membrane-melittin simulations [18].

As shown qualitatively in Figure 1, and quantitatively in Figure 2(A), the melittin peptide was quite stable during the course of the DMPC + Mel simulation in terms of its secondary structure, its orientation relative to the bilayer normal and its depth in the bilayer. We therefore consider the spatial regions within the bilayer where the components of the melittin peptide contributed to the lateral pressure.

Figure 3(A) shows the partial lateral pressures arising from interactions involving three subsections of the melittin peptide; residues 1–11, reffered to as Mel(1–11); residues 12–20, Mel(12–20); and residues 21–26, Mel(21–26). It is somewhat surprising that interactions due to the respective components of melittin were visible well outside the spatial region occupied by those components. In order to establish whether those interactions were due in part to the use of periodic boundary conditions in the simulation along the z direction, a second DMPC + Mel system was constructed with a water layer 20 Å thicker than the one described here. No significant difference was seen in the location or size of the peaks in the pressure profile, indicating that the pressure profile peaks visible in Figure 3 are due to interactions within the membrane and not from interactions with neighboring periodic images.

The most pronounced contribution from the melittin to the pressure profile occurs around $z = 18$ Å, with a large negative peak. This is, of course, consistent with the result of Figure 2, where it was shown that excluding the contribution of melittin to the pressure profile leads to an increase in lateral pressure in the region around $z = 18$ Å. Most of this peak is due to Mel(21–26), which, with its four positively charged side chains near the highly polar lipid headgroups, is well positioned to interact strongly with the bilayer. The other two melittin segments studied here slightly offset the contribution of Mel(21–26) in this region.

Figure 3(B) shows the same total pressure arising from melittin interactions as in Figure 3(A), but instead partitioned by interaction partner rather than by melittin component. A great deal of cancellation between interacting terms is seen, especially between water and headgroups. In particular, melittin gives rise to zero net partial pressures in the region near $z = \pm 25$ Å due to the cancellation of interactions involving water and lipid headgroups. We can observe that the small peaks at $z = -18$ Å and $z = -2$ Å are due to melittin interactions with the lipid tails. Water and headgroup interactions together provide about half the contribution to the large negative peak at $z = 18$ Å, with the rest provided by melittin–tail interactions and a small cancellation due to protein–protein forces.

Figure 3(C) shows how the partial pressures of membrane and water components in DMPC changed upon insertion of melittin. We observe an increase in lateral pressure at $z = 18$ Å where the bilayer and solvent interact with the charged residues in Mel(21–26), and also a small decrease in lateral pressure around $z = -16$ Å. Most strikingly, we see very little change in the solvent region near the upper leaflet due to near perfect cancellation of the change in contribution from headgroup–water interactions with those from headgroup–headgroup and water–water interactions. While headgroup–water interactions are the dominant

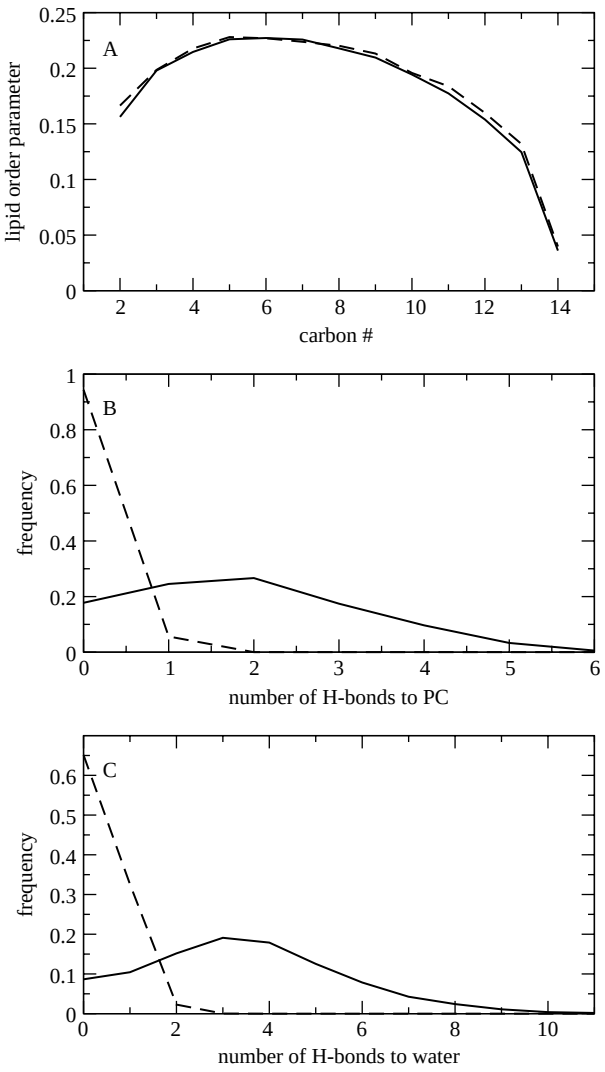

Figure 4. Protein–lipid interactions in DMPC + melittin system. (A) Averaged lipid order parameters of the lower (solid line) and upper (dashed line) leaflets. (B) Fraction of simulation snapshots containing the indicated number of hydrogen bonds with phosphate oxygens for melittin residues 12–20 (dashed line) and 21–26 (solid line). (C) Same as B, but for hydrogen bonds to water.

contributor of surface tension in both simulations, they make a stronger contribution in the presence of melittin; however, headgroup–headgroup and water–water interactions still offset headgroup–water interactions just enough to give nearly zero net change in the tension in the solvent region.

Figure 4(B) and (C) shows the number of hydrogen bonds made by Mel(12–20) and Mel(21–26) with surrounding phosphate groups and water molecules. Mel(1–11), being deeply buried in the hydrophobic portion of the bilayer (Figure 2), made very few hydrogen bonds. Mel(12–20) was found to be hydrogen bonded to phosphate in 5.6% of simulation snapshots, compared to 82% for Mel(21–26). Similarly, Mel(12–20) formed at least one hydrogen bond with water 35% of the time, compared to 91% for Mel(21–26). The difference is, of course, reflected in the proximity of Mel(21–26) to the interface as well as the large number of charged side chains present in Mel(21–26), as compared to Mel(12–20).

4. Discussion

The importance of proteins, small molecules, and other non-lipid components in modulating the hydrophobic environment of lipid bilayers is becoming increasingly well recognized, in part due to recent contributions of molecular simulations. Pressure profile studies of lipids with varying amounts of cholesterol revealed a surprisingly complex pattern of pressure peaks and troughs that varied with cholesterol concentration [12]. Simulations of DPPC over a range of lipid areas (50–80 $\AA^2$/lipid) showed that the tension in the bilayer could be lowered upon addition of trehalose, which is known to stabilize lipid bilayers [29], providing a possible mechanism for the stabilization. Here, we analyzed the lateral pressure of a DMPC bilayer both with and without a melittin peptide, under conditions of nearly identical total surface tension. We find that a single melittin significantly lowers the tension of the lipids surrounding the peptide. The two leaflets of the bilayer exhibit the same surface tension in the peptide-free system, but markedly different tensions when melittin is inserted. The tension in the leaflet containing the amino terminus of the melittin increased by 50% upon melittin insertion, while in the carboxyl terminus the tension decreased by nearly the same amount.

The present work demonstrates that protein–lipid interactions contribute significantly to the total bilayer tension in the vicinity of an inclusion. Additional investigation under conditions of constant surface tension and/or variable lipid number will be required in order to determine how lateral pressure Figures into other modes of protein–lipid interaction, such as the electrostatic potential, in modulating the propensity of peptides to insert into bilayers as well as the equilibrium between conformations of peptide aggregates and integral membrane proteins.

Acknowledgements

This work was supported in part by the National Science Foundation, the National Institutes of Health (GM34921), the Howard Hughes Medical Institute, the National Biomedical Computing Resource, Accelerys, the Keck Foundation, and the Center for Theoretical and Biological Physics.

References

[1] D. Marsh. Lateral pressure in membranes. *Biochimica et Biophysica Acta*, **1286**(3), 183 (1996).
[2] R. Cantor. The influence of membrane lateral pressures on simple geometric models of protein conformational equilibria. *Chem. Phys. Lipids*, **101**(1), 45 (1999).

[3] R.H. Templer, S.J. Castle, A.R. Curran, G. Rumbles, D.R. Klug. Sensing isothermal changes in the lateral pressure in model membranes using di-pyrenyl phosphatidylcholine. *Faraday Discuss.*, **111**, 41 (1998).
[4] G. Brannigan, P.F. Philips, F.L. Brown. Flexible lipid bilayers in implicit solvent. *Phys. Rev. E Stat. Nonlin. Soft. Matter. Phys.*, **72**(1 Pt 1), 011915 (2005).
[5] R. Goetz, R. Lipowsky. Computer simulations of bilayer membranes: self-assembly and interfacial tension. *J. Chem. Phys.*, **108**(17), 7397 (1998).
[6] E. Lindahl, O. Edholm. Spatial and energetic-entropic decomposition of surface tension in lipid bilayers from molecular dynamics simulations. *J. Chem. Phys.*, **113**(9), 3882 (2000).
[7] J. Gullingsrud, K. Schulten. Lipid bilayer pressure profiles and mechanosensitive channel gating. *Biophys. J.*, **86**(6), 3496 (2004).
[8] M.R. de Planque, D.T. Rijkers, R.M. Liskamp, F. Separovic. The alphaM1 transmembrane segment of the nicotinic acetylcholine receptor interacts strongly with model membranes. *Magn. Reson. Chem.*, **42**(2), 148 (2004).
[9] K.L. Martinez, Y. Gohon, P.J. Corringer, C. Tribet, F. Mžrola, J.P. Changeux, J.L. Popot. Allosteric transitions of torpedo acetylcholine receptor in lipids, detergent and amphipols: molecular interactions vs. physical constraints. *FEBS Lett.*, **528**(1-3), 251 (2002).
[10] J.E. Baenziger, M.L. Morris, T.E. Darsaut, S.E. Ryan. Effect of membrane lipid composition on the conformational equilibria of the nicotinic acetylcholine receptor. *J. Biol. Chem.*, **275**(2), 777 (2000).
[11] M. Carrillo-Tripp, S.E. Feller. Evidence for a mechanism by which omega-3 polyunsaturated lipids may affect membrane protein function. *Biochemistry*, **44**(30), 10164 (2005).
[12] M. Patra. Lateral pressure profiles in cholesterol-dppc bilayers. *Eur. Biophys. J.*, 1 (2005).
[13] T. Hessa, H. Kim, K. Bihlmaier, C. Lundin, J. Boekel, H. Andersson, I. Nilsson, S.H. White, G. von Heijne. Recognition of transmembrane helices by the endoplasmic reticulum translocon. *Nature*, **433**, 377 (2005).
[14] C.R. Dawson, A.F. Drake, J. Helliwell, R.C. Hider. The interaction of bee melittin with lipid bilayer membranes. *Biochimica et Biophysica Acta*, **510**(1), 75 (1978).
[15] S. Berneche, M. Nina, B. Roux. Molecular dynamics simulation of melittin in a dimyristoylphosphatidylcholine bilayer membrane. *Biophys. J.*, **75**(4), 1603 (1998).
[16] T.C. Terwilliger, D. Eisenberg. The structure of melittin: structure determination and partial refinement. *J. Biol. Chem.*, **257**(11), 6010 (1982).
[17] W. Humphrey, A. Dalke, K. Schulten. Vmd—visual molecular dynamics. *J. Mol. Graphics*, **14**(1), 33 (1996).
[18] M. Bachar, O.M. Becker. Protein-induced membrane disorder: a molecular dynamics study of melittin in a dipalmitoylphosphatidylcholine bilayer. *Biophys. J.*, **78**, 1359 (2000).
[19] L. Kal, R. Skeel, M. Bhandarkar, R. Brunner, A. Gursoy, N. Krawetz, J. Phillips, A. Shinozaki, K. Varadarajan, K. Schulten. Namd2: greater scalability for parallel molecular dynamics. *J. Comp. Phys.*, **151**(1), 283 (1999).
[20] A.D. MacKerell, D. Bashford, M. Bellott, R.L. Dunbrack, J.D. Evanseck, M.J. Field, S. Fischer, J. Gao, H. Guo, S. Ha, D. Joseph-McCarthy, L. Kuchnir, K. Kuczera, F.T.K. Lau, C. Mattos, S. Michnick, T. Ngo, D.T. Nguyen, B. Prodhom, W.E. Reiher, B. Roux, M. Schlenkrich, J.C. Smith, R. Stote, J. Straub, M. Watanabe, J. Wiorkiewicz-Kuczera, D. Yin, M. Karplus. All-atom empirical potential for molecular modeling and dynamics studies of proteins. *J. Phys. Chem. B*, **102**(18), 3586 (1998).
[21] S.E. Feller, Y.H. Zhang, R.W. Pastor, B.R. Brooks. Constant pressure molecular dynamics simulation—the Langevin piston method. *J. Chem. Phys.*, **103**(11), 4613 (1995).
[22] U. Essmann, L. Perera, M.L. Berkowitz, T. Darden, H. Lee, L.G. Pedersen. A smooth particle mesh Ewald method. *J. Chem. Phys.*, **103**, 8577 (1995).
[23] J.H. Irving, J.G. Kirkwood. The statistical mechanical theory of transport processes. iv. The equations of hydrodynamics. *J. Chem. Phys.*, **18**(6), 817 (1950).
[24] J. Sonne, F.Y. Hansen, GH Peters. Methodological problems in pressure profile calculations for lipid bilayers. *J. Chem. Phys.*, **122**(12), 124903 (2005).
[25] A. Harasima. Molecular theory of surface tension. *Adv. Chem. Phys.*, 203 (1958).
[26] P. Kaszycki, Z. Wasylewski. Fluorescence-quenching-resolved spectra of melittin in lipid bilayers. *Biochimica et Biophysica Acta: Protein Structure and Molecular Enzymology*, **1040**, 337 (1990).
[27] J. Seelig, J.L. Browning. General features of phospholipid conformation in membranes. *FEBS Lett.*, **92**(1), 41 (1978).
[28] S.E. Feller, R.W. Pastor. Constant surface tension simulations of lipid bilayers: the sensitivity of surface areas and compressibilities. *J. Chem. Phys.*, **111**(3), 1281 (1999).
[29] A. Skibinsky, R.M. Venable, R.W. Pastor. A molecular dynamics study of the response of lipid bilayers and monolayers to trehalose. *Biophys. J.*, **89**(6), 4111 (2005).